IEEE Access
Multidisciplinary | Rapid Review | Open Access Journal

Received January 13, 2018, accepted March 4, 2018, date of publication March 12, 2018, date of current version April 18, 2018.

Digital Object Identifier 10.1109/ACCESS.2018.2815148

A Family of Module-Integrated High Step-Up Converters With Dual Coupled Inductors

DONGSHENG YU[1], (Member, IEEE), JIE YANG[2], RUIDONG XU[1], ZHENGLONG XIA[3], HERBERT HO-CHING IU[4], (Senior Member, IEEE), AND TYRONE FERNANDO[4], (Senior Member, IEEE)

[1]School of Electrical and Power Engineering, China University of Mining and Technology, Xuzhou 221116, China
[2]State Grid Linyi Power Supply Company, Linyi 276000, China
[3]School of Electrical Engineering and Automation, Jiangsu Normal University, Xuzhou 221116, China
[4]School of Electrical, Electronic and Computer Engineering, The University of Western Australia, WA 6009, Australia

Corresponding author: Tyrone Fernando (tyrone.fernando@uwa.edu.au)

This work was supported in part by the Key Laboratory of Control of Power Transmission and Conversion, Ministry of Education under Grant 2016AC06, and in part by the Youth Fund of the Foundation Research Project of Jiangsu Province under Grant BK20160219.

ABSTRACT In order to overcome the defect of low output voltage of the renewable energy-based generators, such as the photovoltaic array and fuel cells, a family of high step-up integrated dc/dc converters with dual coupled inductors is proposed based on combination of the modified quadratic boost converters and the voltage-multiplier modules (VMM). The high voltage gain can be achieved by adjusting the duty cycle and turn ratios of the coupled inductor of VMM. In particular, quite low voltage stress on the power switch can be obtained since the switch is no longer directly excited by the high output voltage, which is useful for enlarging the power efficiency. In addition, the two inductors in MQBC are integrated by using one magnetic core to decrease the size of the magnetic components. Very small ripples of the input current can be realized by ripple suppress abilities of the coupled inductors. Two experimental prototypes with rated-power of 200W are selectively constructed for comparative analysis, and experimental results verify the correctness and practicability of the proposed converters.

INDEX TERMS Quadratic boost converters, voltage multiplier module, coupled inductor, integrated converters, low voltage stress.

I. INTRODUCTION

The development of renewable generation has been regarded as an effective method to overcome the global energy crisis and the deterioration of environment [1]–[4]. In general, the output voltage of the renewable energy sources such as fuel cells and PV arrays is relatively low and hence high step-up dc/dc converters are widely required in order to enlarge the DC voltage for supplying the grid-connected inverters and DC loads [5], [6]. Although multitudinous efforts have been dedicated to the design of power converters, new converters with high voltage gain and efficiency are still desirable in consideration of the application scenarios of renewable generation such as fuel cells and photovoltaic systems [7].

Electrical-isolation and high voltage gain are usually together required by industrial application, and hence the transformers based electrical isolated converters have been widely investigated [8]–[14]. The voltage gain of the isolated converters could be adjusted by tuning the turn ratios of the intermediate transformer [8]–[10]. However, improper coupling strength might cause leakage inductance which could result in large voltage spikes on the active switches [11]. Moreover, the isolated converters without continuous and smooth input current could lead to noticeable electromagnetic interference (EMI) [12], [13], and hence bulky input filter is necessarily demanded to properly suppress EMI [14].

In order to achieve high voltage gain, quadratic boost converters (QBCs) are widely utilized, of which the voltage gain can be expressed by a quadratic function in terms of the voltage gain of traditional boost converter [15]–[17]. The QBC presented in [15] is configured by using the traditional topology composed of two cascaded boost converters, while the QBC discussed in [16] is improved on the basis of [15] with low buffer capacitor stress. Recently, the QBCs based on non-cascading structures are newly proposed in [17]. However, the active switch of all the above mentioned QBCs is operated under the stress of high output voltage, and hence the

conduction resistance of the required active switch will result in high-frequency turn-off losses and low energy conversion efficiency [18].

To date, for applications without requirements of electrical isolation, the non-isolated high step-up converters, in virtue of simple structure and small size, have attracted many research attentions [19]–[25]. Switching inductor (SL) and switching capacitor (SC) have been used to structure the high step-up converters, of which the voltage gain mainly relies on the number of voltage lifting units [19], [20]. However, the SL or SC based high step-up converters usually have the drawbacks of large input current fluctuation, weak load regulation and output-voltage stabilizing ability [21], [22]. In order to obtain high voltage conversion without requirement of extreme high duty cycle, the typical boost and SEPIC converters can be modified by introducing the voltage-multiplier cells [23], [24]. However, the voltage gain is dependent on the circuit structure with low adjustable ability [25].

To improve the voltage gain adjustability of boost converters based on voltage-multiplier cells, independent inductors in voltage-multiplier cells can be replaced by the coupled inductors to structure the voltage-multiplier modules (VMM). Then high voltage gain can be obtained by varying the duty cycle as well as the turn ratios of coupled inductors. Also, voltage stress of switching devices can be evidently decreased [7], [26]–[29]. The high voltage gain and low voltage stress across the active switch can also be achieved by combining VMMs and the boost converter [26], [27]. High voltage gain without requiring extreme high duty cycle is achieved by a conventional interleaved boost converter as discussed in [7], by introducing the VMM composed of switched capacitors and coupled inductors. A coupled inductor and two voltage multiplier cells are together employed to obtain high voltage gain in [28]. Moreover, the energy recovery circuit can be naturally formed by the diodes and capacitors and hence the efficiency of the above mentioned converters can be improved. In addition, a high static gain DC-DC converter based on modified SEPIC converter and VMM is proposed in [29], of which the snubbed circuit can be used to minimize the voltage spikes of the active switch.

The VMMs-based high step-up converters comprehensively possessing the high performances of high efficiency, high gain, low voltage stress and continuous input current are still requiring further research attention [30]–[34]. In consideration of extreme high voltage applications, a novel single-switch based high step-up converter has been proposed in [30], which is formed by one QBC and one VMM. By integrating coupled inductor with voltage-multiplier cells, high conversion voltage and low voltage stress of the power devices can be achieved. The three-winding coupled inductor based converter discussed in [31] can also achieve high voltage gain and low voltage stress, which is structured by the improved QBC with low buffer capacitor stress [16] and VMM. A converter is presented in [32] as the alternative power circuit for high voltage conversion and low-to-medium

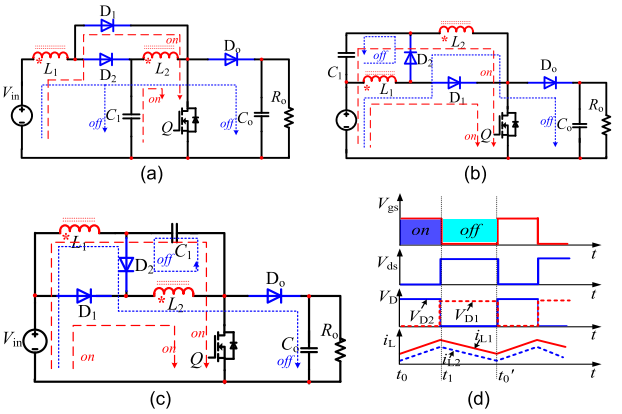

FIGURE 1. Coupled inductor based QBCs and key waveforms. (a) $MQBC_I$. (b) $MQBC_{II}$. (c) $MQBC_{III}$. (d) key waveforms.

power applications, which is built based on the traditional QBC [15] and the coupled inductor based VMM. Hence, the QBCs and VMMs based converters can be used to achieve high voltage gain and low voltage stress [33], [34].

To achieve high efficiency, high voltage gain and low voltage stress, a family of module-integrated converters with high voltage gain by using dual coupled inductors is proposed in this paper. In addition, very small ripples of the input current can also be achieved by the ripple-suppressed ability of coupled inductors. This paper is organized as follows. The circuit topology of the high step-up module-integrated converters is given in Section II. The steady-state operational principles and performances of MQBCI-VMMIII are presented in Section III for demonstration, where the simplified case without considering the loss of leakage inductance is performed to get the static voltage gain and voltage stress. The comparative analysis of steady state performances of MQBC-VMM converters is shown in Section IV, and the experimental results are presented in Section V to validate the theoretical analysis, while conclusions are given in Section VI.

II. DESIGN OF HIGH STEP-UP MODULE-INTEGRATED CONVERTERS

A. THE COUPLED INDUCTORS BASED QBCS

The three modified quadratic boost converters (MQBC) by making use of coupled inductors are shown in Fig.1, labeled as $MQBC_I$, $MQBC_{II}$ and $MQBC_{III}$, respectively. The $MQBC_I$ is derived from the QBC discussed in [15] by coupling inductor L_1 and L_2. The circuits shown in Fig.1 (b) and Fig.1 (c) are derived from $MQBC_I$. During each switching period, MQBCs have two operation stages, and the current path of each stage is indicated by colored dash line in each circuit. The symbols "***on***" and "***off***" beside each dash line represent the time intervals of the switch being turned on and off, respectively. The key waveforms of $MQBC_I$ during one switching period are depicted in Fig.1 (d).

Stage ***on***: The switch Q and diode D_1 are conducted, and the diode D_2 is turned off. The energy of DC source V_{in} is

TABLE 1. A Family of high gain module-integrated converters with single active switch.

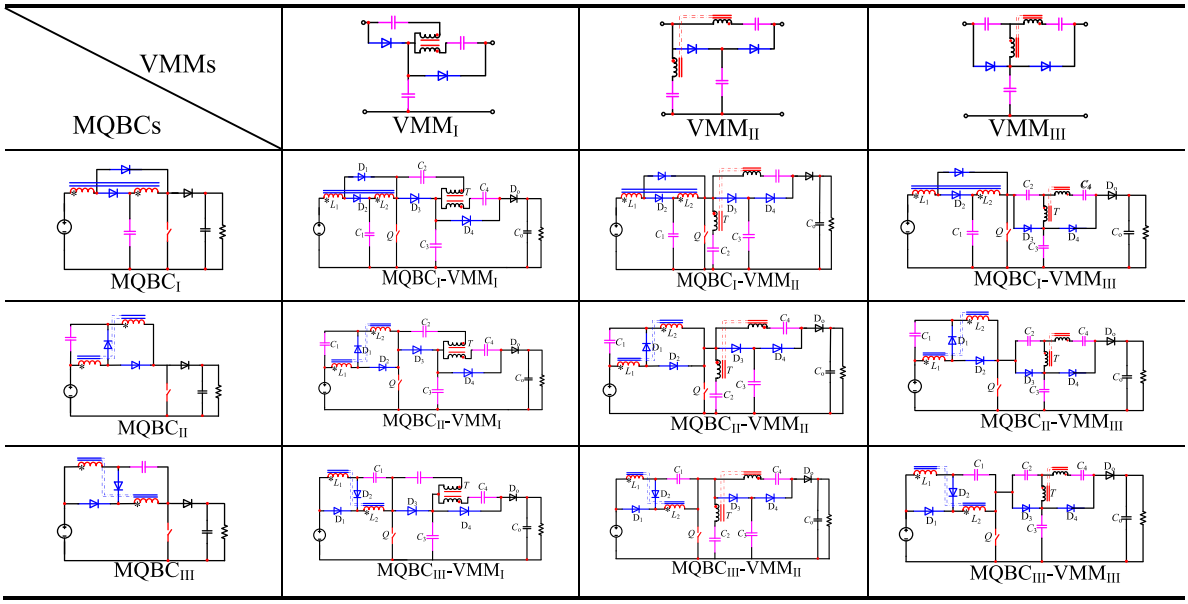

transferred into inductor L_1 through D_1 and Q, and L_2 is charged by capacitor C_1 via Q. Currents passing through L_1 and L_2 are linearly increased.

Stage ***off***: The switch $Q$and diode D_1 are turned off, and the diode D_2 is turned on. The energy stored in $L_1$is released through D_2 to charge C_1, and the energy stored in L_1 and L_2 is supplied to the load at the same time. Currents going through L_1 and L_2 are linearly declined.

Based on the volt-second balance principle of $L_1$and L_2, the gain expression of these three MQBCs can be presented by

$$G(D) = \frac{1}{(1-D)^2} \tag{1}$$

where D is the control duty-cycle of switch Q.

B. VOLTAGE MULTIPLIER MODULES

Three circuit structures of VMM are presented in Fig.2, labeled as VMM$_{I}$, VMM$_{II}$ and VMM$_{III}$, respectively, where $T$is a coupled inductor with primary and the secondary windings denoted by n_p and n_s, respectively. The voltage gains of VMMs can be calculated as

$$G_{\mathrm{VMM_I}} = 1 + N, \quad G_{\mathrm{VMM_{II}}} = G_{\mathrm{VMM_{III}}} = 2 + N \tag{2}$$

where N is the turn ratios of the coupled inductor T. Evidently, the voltage gain of VMM can be adjusted by tuning the turn ratios of the coupled inductors.

C. DERIVATION OF THE MODULE-INTEGRATED CONVERTERS

The voltage gain of MQBCs is only decided by the duty cycle of control signal. Therefore, for the applications required very high voltage gain, the duty cycle might be adjusted to extremely high value and the active switch is then performed under high voltage stress. A family of high step-up converters is proposed by the combination of MQBC and VMM in order to obtain higher voltage gain and lower voltage stress on power devices, as shown in Table 1. Nine coupled inductors based converters with high gain can be obtained.

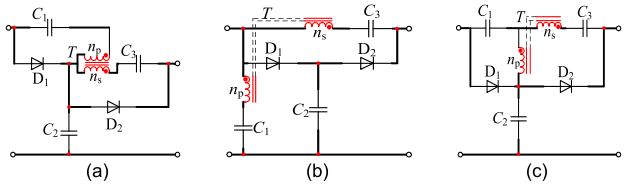

FIGURE 2. VMM$_s$ with coupled inductors. (a) VMM$_I$. (b) VMM$_{II}$. (c) VMM$_{III}$.

Evidently, the proposed module-integrated converters can achieve higher voltage gain for given duty cycles as compared to single MQBC or VMM based converters since the voltage gain can be controlled both by duty cycle and the turn ratios of coupled inductor.

III. DEMONSTRATIVE ANALYSIS OF MQBC$_I$-VMM$_{III}$

To further analyze the steady-state operation performance of the proposed converter family, the converter structured by MQBC$_I$ and VMM$_{III}$ is selected as illustrative example for theoretical discussion.

A. CIRCUIT TOPOLOGY

To improve the power density, the inductors L_1 and L_2 of MQBC$_I$ could be assembled into one magnetic core to structure the coupled inductor T_1, which will reduce the size of magnetic components. Very small ripples of the input current can be achieved in virtue of the ripple-suppressed

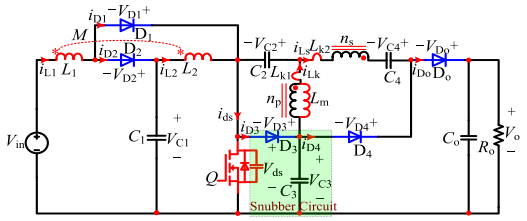

FIGURE 3. Equivalent circuit of $MQBC_I$-VMM_{III}.

ability of the coupled inductors. The equivalent circuit of the $MQBC_I$-VMM_{III} converter is shown in Fig.3, of which D_1, D_2 and D_4 are freewheeling diodes, D_3 and D_o are the clamp diodes, respectively. C_o is the output filter capacitor, while T_1 and T_2 are the coupled inductors. One attractive advantage of this proposed converter is the snubber circuit naturally structured by D_3 and C_3 of VMM_{III}, as shown inside the dotted frame. This snubbed circuit is capable of reducing the voltage spikes on power switch Q possibly caused by leakage inductance. The mutual inductance and the turn ratios ofT_1 are presented by M and N_1, respectively. T_2 is operated under high frequency and can be equalized as a magnetizing inductor L_m in connection with leakage inductor L_{k1} and L_{k2}.

For analysis simplification, T_2 is equalized as an ideal transformer with the coupling coefficient $k_2 = L_m/(L_m+L_{k1})$ and the turn ratio $N_2 = n_s/n_p$. The operation stages of the demonstrative converter $MQBC_I$-VMM_{III} are shown in Fig.4. The operation stages during one switching period can be described as follows.

1) STAGE 1

The switch Q is conducted, while Diodes D_2, D_3 and D_o are turned off and diodes D_1 and D_2 are turned on. The energy from DC source V_{in} is delivered to L_1 by D_1 and Q, and L_2 is charged by C_1 via Q. Currents i_{L1} and i_{L2} are linearly enlarged. C_3 is discharged and the energy is released to inductor L_m and C_2 via Q, which results in the increment of current i_{Lk}; the energy stored in the secondary winding of T_2 is released to C_4. Hence, we have

$$L_1\frac{di_{L1}}{dt} + M\frac{di_{L2}}{dt} = V_{in} \tag{3}$$

$$M\frac{di_{L1}}{dt} + L_2\frac{di_{L2}}{dt} = V_{C1} \tag{4}$$

$$V_{ns} = V_{C2} + V_{C4} - V_{C3} \tag{5}$$

where V_{ns} is the voltage across the secondary winding of T_2.

2) STAGE 2

The switch Q, D_1 and D_o are turned off, while D_3 is conducted. The energy stored in L_1 is released through D_2 to charge capacitor C_1, and the current i_{L1} is linearly declined; the energy stored in L_2 is transferred to C_3 via D_3. The current i_{L2} going through Q is quickly decreased by D_3. The voltage stress on Q is equal to V_{C3} due to the conduction of D_3, and the snubbed circuit composed of D_3 and C_3 can

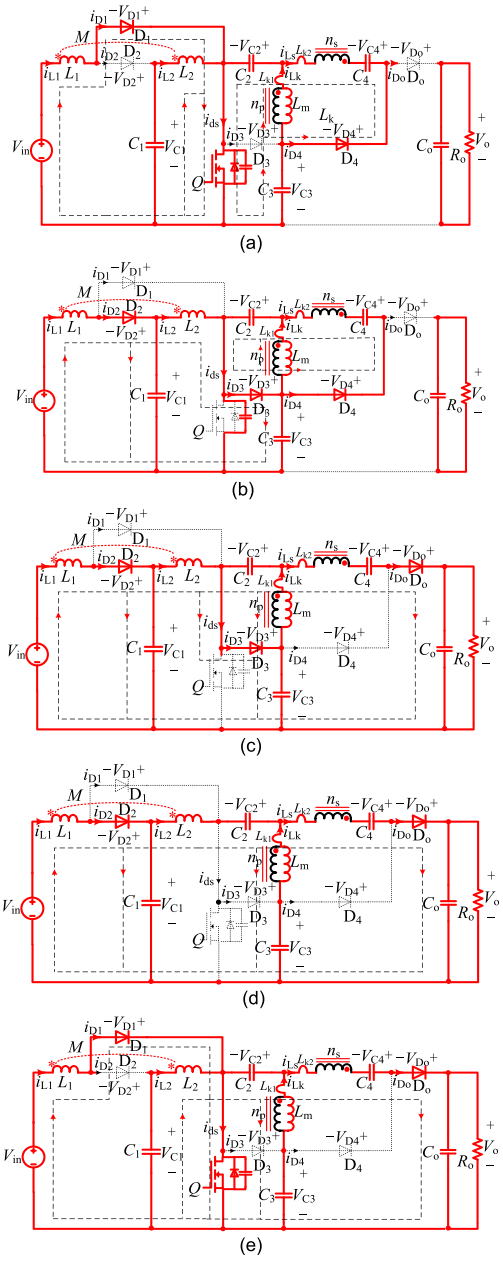

FIGURE 4. Equivalent circuits of five operation stages during a switching period. (a) Stage 1. (b) Stage 2. (c) Stage 3. (d) Stage 4. (e) Stage 5.

be naturally formed in virtue of the parallel capacitor of Q, which could reduce the voltage spikes on Q during the transient operation between stages. The energy stored in L_{k1} is discharged through D_3 and then the energy is stored in capacitor C_2, which leads to the linear decrement of i_{Lk}. Meanwhile, the energy stored in L_{k2} is transferred to C_4 by the energy recovery circuit consisting of D_3, D_4 and C_4. The following equations hold,

$$V_{ns} = V_{C2} + V_{C4}, \quad V_{ds} = V_{C3} \tag{6}$$

$$L_{k1}\frac{di_{Lk1}}{dt} = -V_{C2} - \frac{V_{C2}+V_{C4}}{N_2} \tag{7}$$

3) STAGE 3

Q is remained off and the current $-i_{Ls}$ is decreased to zero. D_4 is turned off and D_o is conducted. L_1 and L_2 are discharged and the energy is delivered to capacitorsC_1 and C_3. Also, the energy is transported to supply the load by the circuit loop consisting of C_2, the secondary side of T_2, C_4 and D_o. Thus, the currents i_{L1} and i_{L2} are still linearly declined, and the leakage inductance currents $-i_{Lk}$ and i_{Ls} are increased. We have

$$L_1\frac{di_{L1}}{dt}+M\frac{di_{L2}}{dt}=V_{in}-V_{C1} \tag{8}$$

$$M\frac{di_{L1}}{dt}+L_2\frac{di_{L2}}{dt}=V_{C1}-V_{C3} \tag{9}$$

$$V_{ns}=V_{C2}+V_{C4}-(V_o-V_{C3}) \tag{10}$$

$$L_{k1}\frac{di_{Lk1}}{dt}=-V_{C2}-\frac{V_{C2}+V_{C4}-(V_o-V_{C3})}{N_2} \tag{11}$$

4) STAGE 4

The switch Q remains off. D_3 can achieve zero-current turn-off and its voltage stress is equal to the summation of V_{C2} and V_{Lm}. Therefore, the voltage stress on Q can be decreased to V_{C3}-V_{C2}-V_{Lm}. Namely,

$$V_{D3}=V_{C2}+V_{Lm} \tag{12}$$

$$V_{ds}=V_{C3}-V_{C2}-V_{Lm} \tag{13}$$

In addition, the currents i_{L1} and i_{L2} are still linearly decreased and the current $-i_{Lk}$ is also declined.

5) STAGE 5

The switch Q is turned on. L_1 is charged by V_{in} and L_2 is excited by V_{C1}. The currents i_{L1} and i_{L2} are linearly increased. Meanwhile, the energy stored in L_m and C_2 is released to charge C_3, and the secondary side of T_2 is supplying energy to the load. Therefore, the currents $-i_{Lk}$ and i_{Ls} are declined. The voltage on leakage inductance L_{k1} can be represented as follows,

$$L_{k1}\frac{di_{Lk1}}{dt}=V_{C3}-V_{C2}-\frac{V_{ns}}{N_2} \tag{14}$$

After the currents $-i_{Lk}$ and i_{Ls} are reduced to zero, the next switching period is initialized.

B. VOLTAGE GAIN OF MQBC$_I$-VMM$_{III}$

During the stage 1 as shown in Fig.4 (a), L_1, L_2 and L_m are charged and the voltages across inductors can be expressed by

$$\begin{bmatrix}V_{L1}\\V_{L2}\end{bmatrix}=\begin{bmatrix}L_1 & M\\M & L_2\end{bmatrix}\begin{bmatrix}\frac{di_{L1}}{dt}\\\frac{di_{L2}}{dt}\end{bmatrix}=\begin{bmatrix}V_{in}\\V_{C1}\end{bmatrix} \tag{15}$$

$$V_{Lm}=\frac{V_{C2}+V_{C4}-V_{C3}}{N_2}=k_2(V_{C3}-V_{C2}) \tag{16}$$

For the stage 3 as shown in Fig.4 (c), the switch $Q$is turned off. L_1, L_2 and L_m are hence discharged, namely

$$\begin{bmatrix}V_{L1}\\V_{L2}\end{bmatrix}=\begin{bmatrix}L_1 & M\\M & L_2\end{bmatrix}\begin{bmatrix}\frac{di_{L1}}{dt}\\\frac{di_{L2}}{dt}\end{bmatrix}=\begin{bmatrix}V_{in}-V_{C1}\\V_{C1}-V_{C3}\end{bmatrix} \tag{17}$$

$$V_{Lm}=\frac{V_{C2}+V_{C4}-(V_o-V_{C3})}{N_2}=-k_2V_{C2} \tag{18}$$

Applying the volt-second balance principle to the inductors L_1, L_2 and L_m, we have

$$\int_0^{DT_s}V_{in}dt+\int_{DT_s}^{T_s}(V_{in}-V_{C1})dt=0 \tag{19}$$

$$\int_0^{DT_s}V_{C1}dt+\int_{DT_s}^{T_s}(V_{C1}-V_{C3})dt=0 \tag{20}$$

$$\int_0^{DT_s}k_2(V_{C3}-V_{C2})dt+\int_{DT_s}^{T_s}k_2(-V_{C2})dt=0 \tag{21}$$

$$\int_0^{DT_s}(\frac{V_{C2}+V_{C4}-V_{C3}}{N_2})dt+\int_{DT_s}^{T_s}k_2(-V_{C2})dt=0 \tag{22}$$

Based on (17)-(22), the voltages across C_1, C_2, C_3 and C_4 can be derived by

$$V_{C1}=\frac{1}{1-D}V_{in},\quad V_{C2}=\frac{D}{(1-D)^2}V_{in} \tag{23}$$

$$V_{C3}=\frac{1}{(1-D)^2}V_{in},\quad V_{C4}=\frac{1+k_2N_2}{1-D}V_{in} \tag{24}$$

According to (16) and (21)-(24), the output voltage of MQBC$_I$-VMM$_{III}$ can be expressed by

$$V_o=(1+k_2N_2)V_{C2}+V_{C3}+V_{C4}=\frac{2+k_2N_2}{(1-D)^2}V_{in} \tag{25}$$

Hence, the voltage gain of MQBC$_I$-VMM$_{III}$ can be written by,

$$G(D,N_2,k_2)=\frac{V_o}{V_{in}}=\frac{2+k_2N_2}{(1-D)^2} \tag{26}$$

It can be observed from (26) that, the voltage gain of the MQBC$_I$-VMM$_{III}$ is decided by the duty cycle D, the turn ratios N_2 and coupling coefficientk_2. Since the influence from leakage inductance can be ignored due to its relatively small value as compared with L_m. Then, the voltage gain of the MQBC$_I$-VMM$_{III}$ can be rewritten as,

$$G(D,N_2)_{CCM}=\frac{V_o}{V_{in}}=\frac{2+N_2}{(1-D)^2} \tag{27}$$

The voltage gain curves of MQBC$_I$-VMM$_{III}$ in terms of D are presented in Fig.5, as N_2 is equal to 1, 2 and 3 and k_2 is equal to 1. Evidently, for a given duty cycle value, the voltage gain of MQBC$_I$-VMM$_{III}$ converter is higher than QBC$_I$ and the higher gain can also be achieved by increasing the turns ratio N_2.

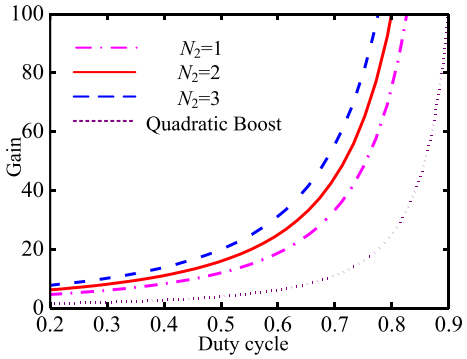

FIGURE 5. Voltage gain comparison of MQBCI-VMM$_{III}$ in terms of N_2.

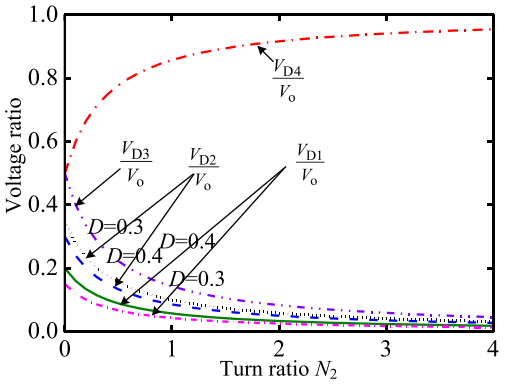

FIGURE 6. Ratios between diode voltage and output voltage with different N_2 and D.

C. VOLTAGE AND CURRENT STRESS ANALYSIS

According to the preceding analysis of voltage gain and by neglecting the influence from leakage inductance and the voltage ripples acrossC_3, the maximum voltage stress on the power switch can be derived by

$$V_{Q,\text{stress}} = \frac{1}{(1-D)^2}V_{\text{in}} = \frac{1}{2+N_2}V_{\text{o}} \tag{28}$$

The voltage stresses of the diodes can be written by

$$V_{\text{D1,stress}} = \frac{D}{(1-D)^2}V_{\text{in}} = \frac{D}{2+N_2}V_{\text{o}} \tag{29}$$

$$V_{\text{D2,stress}} = \frac{1}{1-D}V_{\text{in}} = \frac{1-D}{2+N_2}V_{\text{o}} \tag{30}$$

$$V_{\text{D3,stress}} = \frac{1}{(1-D)^2}V_{\text{in}} = \frac{1}{2+N_2}V_{\text{o}} \tag{31}$$

$$V_{\text{D4,stress}} = \frac{1+N_2}{(1-D)^2}V_{\text{in}} = \frac{1+N_2}{2+N_2}V_{\text{o}} \tag{32}$$

$$V_{\text{Do,stress}} = \frac{1+N_2}{(1-D)^2}V_{\text{in}} = \frac{1+N_2}{2+N_2}V_{\text{o}} \tag{33}$$

The ratio between the diode voltage and the output voltage in terms of different N_2 and D is exhibited by Fig.6. It is noticeable that the ratio between the voltage across $D_1 \sim D_3$ and the output voltage can be decreased by the increment of N_2. Nevertheless, the ratio between V_{D4} and V_{o} can be enlarged by increasing N_2. In addition, the ratio between the voltage across $D_1 \sim D_2$ and the output voltage is also decided by the value of duty cycle D. The value of $V_{\text{D1}}/V_{\text{o}}$ can be decreased by increasing N_2 and D. Hence, the duty cycle and the turn ratios should be comprehensively configured in order to achieve low voltage stress and switching losses.

The current ripples on the inductors L_1, L_2 and L_{m} can be expressed by

$$\Delta I_{\text{L1}} = \frac{(L_2V_{\text{in}} - MV_{\text{C1}})D}{(L_1L_2 - M^2)f_{\text{s}}}, \quad \Delta I_{\text{L2}} = \frac{(L_1V_{\text{C1}} - MV_{\text{in}})D}{(L_1L_2 - M^2)f_{\text{s}}}, \tag{34}$$

where mutual inductance $M = k_1\,(L_1L_2)^{1/2}$.

$$\Delta I_{\text{Lm}} = \frac{V_{\text{in}}}{(1-D)L_{\text{m}}}DT_{\text{s}}. \tag{35}$$

By analyzing Fig.6 (a) and Fig.6 (b), the peak current of diodes D_1 and D_2 can be derived by

$$I_{\text{D1}}(\text{peak}) = \frac{2+N_2}{(1-D)^2}I_{\text{o}} + \frac{\Delta I_{\text{L1}}}{2}, \tag{36}$$

$$I_{\text{D2}}(\text{peak}) = \frac{2+N_2}{(1-D)^2}I_{\text{o}} + \frac{\Delta I_{\text{L1}}}{2}. \tag{37}$$

Since the average values of the currents passing through C_2, C_3, C_4 during one switching period are zero, by applying the Ampere-second balance principle to C_2, C_3 and C_4, the average currents flowing through D_3, D_4 and D_{o} are equal to the average value of i_{o}. The current stresses on D_3, D_4, D_{o} and the power switch Q can be obtained by

$$I_{\text{D3}}(\text{peak}) = \frac{2I_{\text{o}}}{D} + \frac{V_{\text{in}}}{2(1-D)L_{\text{m}}}DT_{\text{s}}, \tag{38}$$

$$I_{\text{D4}}(\text{peak}) = \frac{2}{D}I_{\text{o}}, \quad I_{\text{Do}}(\text{peak}) = \frac{2}{1-D}I_{\text{o}} \tag{39}$$

$$I_Q(\text{peak}) = \frac{2(1-D)}{D}I_{\text{L1}} + \frac{\Delta I_{\text{L1}}}{2}. \tag{40}$$

D. ZERO RIPPLE OF INPUT CURRENT

Very small ripples of the input current can be achieved due to the ripple-suppressed abilities of the coupled inductor. Based on (34), the input current characterized by zero ripples can be achieved when the ΔI_{L1} is reduced to zero. Hence, the following equations can be derived,

$$\Delta I_{\text{L1}} = \frac{(L_2V_{\text{in}} - MV_{\text{C1}})D}{(L_1L_2 - M^2)f_{\text{s}}} = 0 \Rightarrow L_2V_{\text{in}} - MV_{\text{C1}} = 0 \tag{41}$$

For steady-state operation, by substituting (23) into (41), we have

$$M = (1-D)L_2 \tag{42}$$

Hence, the conditions to achieve zero input-current ripples can be obtained by,

$$k_1 = (1-D)\sqrt{\frac{L_2}{L_1}} < 1 \tag{43}$$

TABLE 2. Performance comparison of QBC-VMM converters.

	$MQBC_I$			$MQBC_{II}$			$MQBC_{III}$		
	$MQBC_I$-VMM_I	$MQBC_I$-VMM_{II}	$MQBC_I$-VMM_{III}	$MQBC_{II}$-VMM_I	$MQBC_{II}$-VMM_{II}	$MQBC_{II}$-VMM_{III}	$MQBC_{III}$-VMM_I	$MQBC_{III}$-VMM_{II}	$MQBC_{III}$-VMM_{III}
Voltage gain	$\frac{1+N_2}{(1-D)^2}$	$\frac{2+N_2}{(1-D)^2}$	$\frac{2+N_2}{(1-D)^2}$	$\frac{1+N_2}{(1-D)^2}$	$\frac{2+N_2}{(1-D)^2}$	$\frac{2+N_2}{(1-D)^2}$	$\frac{1+N_2}{(1-D)^2}$	$\frac{2+N_2}{(1-D)^2}$	$\frac{2+N_2}{(1-D)^2}$
Voltage stress on Q	$\frac{V_o}{1+N_2}$	$\frac{V_o}{2+N_2}$	$\frac{V_o}{2+N_2}$	$\frac{V_o}{1+N_2}$	$\frac{V_o}{2+N_2}$	$\frac{V_o}{2+N_2}$	$\frac{V_o}{1+N_2}$	$\frac{V_o}{2+N_2}$	$\frac{V_o}{2+N_2}$
Current stress of Q	$\frac{I_{in}}{D}$	$\frac{2I_{in}(1-D)}{D}$	$\frac{2I_{in}(1-D)}{D}$	$\frac{I_{in}}{D}$	$\frac{2I_{in}(1-D)}{D}$	$\frac{2I_{in}(1-D)}{D}$	$\frac{I_{in}}{D}$	$\frac{2I_{in}(1-D)}{D}$	$\frac{2I_{in}(1-D)}{D}$
Input current ripple	Small	Small	Small	Large	Large	Large	Large	Large	Large
Voltage stress of D_1	$\frac{DV_o}{1+N_2}$	$\frac{DV_o}{2+N_2}$	$\frac{DV_o}{2+N_2}$	$\frac{(1-D)V_o}{1+N_2}$	$\frac{(1-D)V_o}{2+N_2}$	$\frac{(1-D)V_o}{2+N_2}$	$\frac{DV_o}{1+N_2}$	$\frac{DV_o}{2+N_2}$	$\frac{DV_o}{2+N_2}$
Voltage stress of D_2	$\frac{(1-D)V_o}{1+N_2}$	$\frac{(1-D)V_o}{2+N_2}$	$\frac{(1-D)V_o}{2+N_2}$	$\frac{DV_o}{1+N_2}$	$\frac{DV_o}{2+N_2}$	$\frac{DV_o}{2+N_2}$	$\frac{(1-D)V_o}{1+N_2}$	$\frac{(1-D)V_o}{2+N_2}$	$\frac{(1-D)V_o}{2+N_2}$
Voltage stress of D_3	$\frac{V_o}{1+N_2}$	$\frac{V_o}{2+N_2}$	$\frac{V_o}{2+N_2}$	$\frac{V_o}{1+N_2}$	$\frac{V_o}{2+N_2}$	$\frac{V_o}{2+N_2}$	$\frac{V_o}{1+N_2}$	$\frac{V_o}{2+N_2}$	$\frac{V_o}{2+N_2}$
Voltage stress of D_4	$\frac{N_2V_o}{1+N_2}$	$\frac{(1+N_2)V_o}{2+N_2}$	$\frac{(1+N_2)V_o}{2+N_2}$	$\frac{N_2V_o}{1+N_2}$	$\frac{(1+N_2)V_o}{2+N_2}$	$\frac{(1+N_2)V_o}{2+N_2}$	$\frac{N_2V_o}{1+N_2}$	$\frac{(1+N_2)V_o}{2+N_2}$	$\frac{(1+N_2)V_o}{2+N_2}$
Voltage stress of D_o	$\frac{N_2V_o}{1+N_2}$	$\frac{(1+N_2)V_o}{2+N_2}$	$\frac{(1+N_2)V_o}{2+N_2}$	$\frac{N_2V_o}{1+N_2}$	$\frac{(1+N_2)V_o}{2+N_2}$	$\frac{(1+N_2)V_o}{2+N_2}$	$\frac{N_2V_o}{1+N_2}$	$\frac{(1+N_2)V_o}{2+N_2}$	$\frac{(1+N_2)V_o}{2+N_2}$
Average current of D_o	I_o	I_o	I_o	I_o	I_o	I_o	I_o	I_o	I_o
Voltage stress of C_1	$\frac{(1-D)V_o}{1+N_2}$	$\frac{(1-D)V_o}{2+N_2}$	$\frac{(1-D)V_o}{2+N_2}$	$\frac{D(1-D)V_o}{1+N_2}$	$\frac{D(1-D)V_o}{2+N_2}$	$\frac{D(1-D)V_o}{2+N_2}$	$\frac{D(1-D)V_o}{1+N_2}$	$\frac{D(1-D)V_o}{2+N_2}$	$\frac{D(1-D)V_o}{2+N_2}$
Snubber circuit	D_3 C_3	None	D_3 C_3	D_3 C_3	None	D_3 C_3	D_3 C_3	None	D_3 C_3
Recovery circuit	C_4 D_4	C_4 D_3 D_4	C_4 D_3 D_4	C_4 D_4	C_4 D_3 D_4	C_4 D_3 D_4	C_4 D_4	C_4 D_3 D_4	C_4 D_3 D_4

The input current characterized by very small ripples close to zero can be achieved by suitably configuring the coupling coefficient of T_1 to satisfy (43). It should be noted that the voltage gain of the proposed converters is independent of the coupling coefficient k_1. In other words, high voltage gain can be achieved no matter L_1 and L_2 are independent or coupled by the same magnetic core. To realize the input current with very small ripples, the required value of L_2 should be larger than the critical value to ensure CCM operation.

IV. COMPARATIVE ANALYSIS OF MQBC-VMM CONVERTERS

The methods used for analyzing converter $MQBC_I$-VMM_{III} can be applied to the rest eight cases of MQBC-VMM converters listed in Table 1. The theoretical calculation results are shown in Table 2 for comparatively analyzing this converter family. It can be observed from Table 2 that the voltage gain of MQBC-VMM is in fact equivalent to the product of the voltage gains of MQBC and VMM. This result also verifies that the gain of MQBC-VMM converter can be controlled by the duty cycle of MQBC and the turn ratios of the coupled inductor inside VMM, namely,

$$G_{\text{QBC-VMM}} = G_{\text{QBC}} G_{\text{VMM}} \tag{44}$$

According to Table 2, the converters structured by $MQBC_I$ can achieve small ripples of input current in virtue of the ripple-suppressed ability of the coupled inductor. For the converters containing $MQBC_{II}$ and $MQBC_{III}$, the voltage stress across the buffer capacitor C_1 is relatively low and buffer capacitors with small parasitic resistance can be utilized in order to reduce power losses and overall size. Also, the snubbed circuits can be naturally formed in the MQBC-VMM converters by VMM_1 and VMM_{III} and hence the voltage spikes on the power switch can be decreased. In addition, the whole family of MQBC-VMM converters can structure an energy recovery circuit by making use of the diodes and capacitors inside the VMM, by virtue of which, the leakage inductive energy can be recovered and delivered to the load.

The performance of converters with high voltage gain structured by coupled inductors are comparatively listed in Table 3, from which we can see that, the converter proposed in [26] with fewer switching devices can achieve high gain and low losses of leakage inductance. The high gain converter with dual switches proposed in [27] can obtain lower voltage stress on the switching devices, but based on high complexities of control process. The proposed converters MQBC-VMM and the converters presented in [33] and [34] can achieve higher voltage gain by integrating the QBC

TABLE 3. Performance comparison of the prototypes.

Converters	[26]	[27]	[33]	[34]	$MQBC_{I,II,III}$ -VMM_{I}	$MQBC_{I,II,III}$ -$VMM_{II,III}$
Number of switch	1	2	1	1	1	1
Number of diode	3	4	5	4	5	5
Voltage gain in CCM	$\frac{2+N}{1-D}$	$\frac{2+2N}{1-D}$	$\frac{1+2N(1-D)}{(1-D)^2}$	$\frac{1+ND}{(1-D)^2}$	$\frac{1+N_2}{(1-D)^2}$	$\frac{2+N_2}{(1-D)^2}$
Voltage stress on switch	$\frac{V_o}{2+N}$	$\frac{V_o}{2+2N}$	$\frac{V_o}{1+2N(1-D)}$	$\frac{V_o}{1+ND}$	$\frac{V_o}{1+N_2}$	$\frac{V_o}{2+N_2}$
Maximum voltage stress on diodes	$\frac{(1+N)V_o}{2+N}$	$\frac{(1+N)V_o}{2+2N}$	$\frac{NV_o}{1+2N(1-D)}$	$\frac{NV_o}{1+ND}$	$\frac{N_2V_o}{1+N_2}$	$\frac{(1+N_2)V_o}{2+N_2}$
Leakage inductance loss	Small	Large	Large	Large	Small	Small
Reverse recovery loss	Small	Small	Medium	Medium	Small	Small

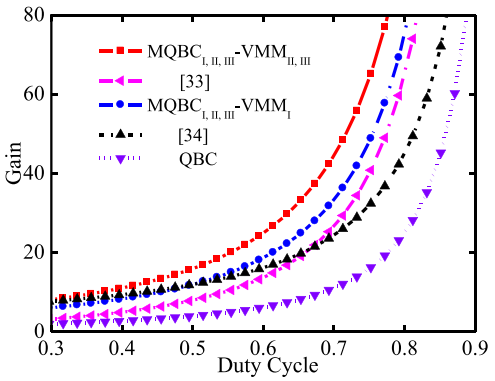

FIGURE 7. Voltage gain comparison of the proposed converter, the conventional quadratic boost and reference [33], [34] with $N_2 = n = 2$.

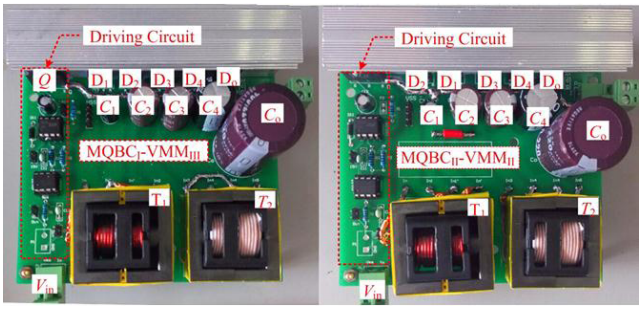

FIGURE 8. Experimental prototypes of proposed converters $MQBC_I$-VMM_{III} and $MQBC_{II}$-VMM_{II}.

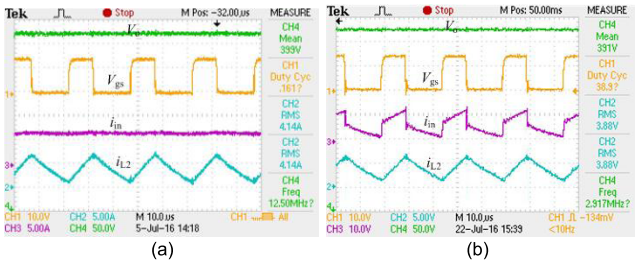

FIGURE 9. Measured waveforms of V_{gs}, i_{in}, i_{L2} and V_o when $V_{in} = 36V$. (a) $MQBC_I$-VMM_{III}. (b) $MQBC_{II}$-VMM_{II}.

and coupled-inductors. However, in addition to higher voltage gain, the MQBC-VMM module-integrated converters can achieve quite low voltage stress of the active switch and diodes as well as small reverse recovery loss in the output diode, as compared with the converters presented in [33] and [34].

V. EXPERIMENTAL TESTS OF THE PROPOSED CONVERTERS

For comprehensively presenting the operation performance of this converter family, $MQBC_I$-VMM_{III} and $MQBC_{II}$-VMM_{II} are illustratively selected for laboratory tests. The parameters of the converter prototype are configured as V_{in} = 18V∼36V, V_o = 400V, P_o = 200W, f_s = 40 kHz, N_1 = 25:15, $L_1 = 207\mu$H, $L_2 = 98\mu$H, $M = 45$uH; $N_2 = 45:15$, $L_m = 250\mu$H, $L_k = 1.2\mu$H; $C_1 = C_2 = C_3 = C_4 = 47\mu$F, $C_o = 220\mu$F

The experimental prototypes of $MQBC_I$-VMM_{III} and $MQBC_{II}$-VMM_{II} are shown in Fig.8. The measured waveforms of the control signal Q, the output voltage, the input current i_{in} and the current i_{L2} are shown in Fig.9, respectively. It can be seen that, the ripples of the input current i_{in} of $MQBC_I$-VMM_{III} can be decreased to lower than 5% of the average input current, while the current i_{in} of $MQBC_{II}$-VMM_{II} is continuous but with the ripples up to 50% of the average current. Also, the currents going through L_2 of $MQBC_I$-VMM_{III} and $MQBC_{II}$-VMM_{II} are continuous.

The control signal of Q, the voltage V_{ds} and currents i_{ds} and i_{D3} of $MQBC_I$-VMM_{III} and $MQBC_{II}$-VMM_{II} are exhibited in Fig.10, from which we can see that, once D_3 is conducted, the snubber circuit formed by D_3, C_3 and the parasitic capacitance of Q can be automatically activated for suppressing the voltage spikes. When D_3 is switched off, the voltage across $Q$is then reduced from V_{C3} to the value of V_{C3}-V_{C2}-V_{Lm}. Comparatively, large voltage spikes can be detected in Q of $MQBC_{II}$-VMM_{II} since no snubbed circuit is naturally formed in VMM_{II}.

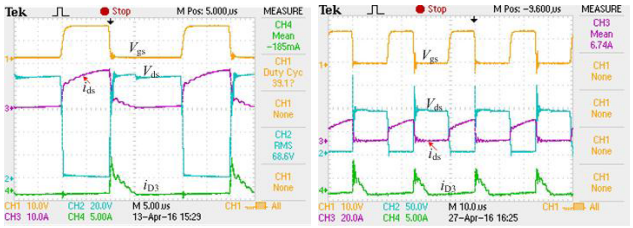

FIGURE 10. Experimental waveforms of V_{gs}, V_{ds}, i_{ds} and i_{D3}. (a) MQBC$_{I}$-VMM$_{III}$. (b) MQBC$_{II}$-VMM$_{II}$.

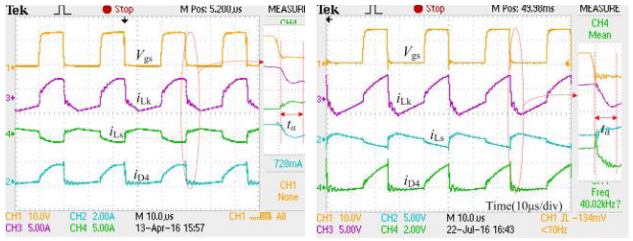

FIGURE 11. Experimental waveforms of i_{Lk}, i_{Ls} and i_{D4}. (a) MQBC$_{I}$-VMM$_{III}$. (b) MQBC$_{II}$-VMM$_{II}$.

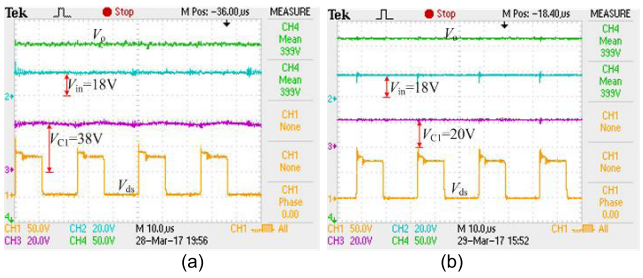

FIGURE 12. Experimental waveforms of V_{in}, V_{ds}, V_{C1} and V_{C3}. (a) MQBC$_{I}$-VMM$_{III}$. (b) MQBC$_{II}$-VMM$_{II}$.

The control signal of Q, the current waveforms including i_{Lk}, i_{Ls} and i_{D4} of MQBC$_{I}$-VMM$_{III}$ and MQBC$_{II}$-VMM$_{II}$ are displayed in Fig.11, respectively. It can be observed that, at the beginning of stage 2, switch Q is turned-off, the current going through D_4 commences to decline and diode D_3 is conducted. During the time interval t_α, the energy stored in leakage inductor L_{k1} can be transferred to C_2 and the energy stored in L_{k2} is firstly released toC_4 by the energy recovery circuit composed of D_3, D_4 and C_4, and then to the load.

The voltages across Q and C_1, the input and the output voltage of MQBC$_{I}$-VMM$_{III}$ and MQBC$_{II}$-VMM$_{II}$ are shown in Fig.12, respectively. The voltage across C_1 of MQBC$_{I}$-VMM$_{III}$ is measured as 38V and the output voltage steadily reaches 400V, while the voltage stress of C_1 in MQBC$_{II}$-VMM$_{II}$ is detected as 20V. These results reveal that MQBC$_{I}$-VMM$_{III}$ possesses higher voltage stress as compared with MQBC$_{II}$-VMM$_{II}$. These experimental results are in good agreement with the theoretical analysis.

The experimentally sampled efficiency curves of MQBC$_{I}$-VMM$_{III}$ and MQBC$_{II}$-VMM$_{II}$ are depicted in Fig.13 (a).

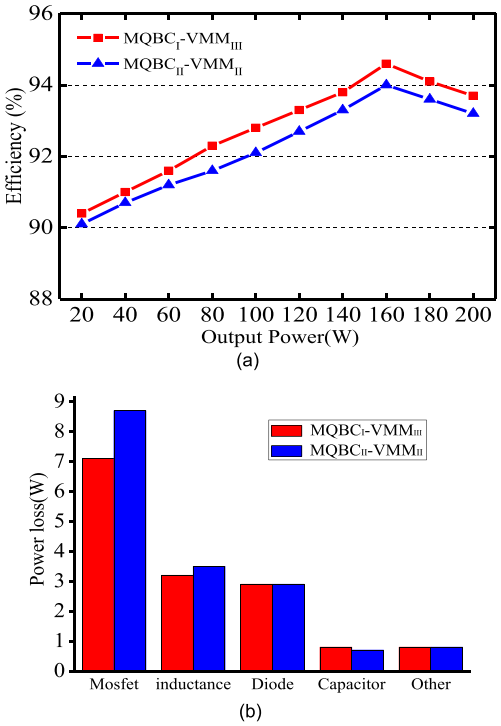

FIGURE 13. Experimental results of the converter efficiency and the total power loss. (a) Converter efficiency (b) Power loss with 200W load.

The efficiency of MQBC$_{I}$-VMM$_{III}$ is measured as 93.7% when the converter is fully loaded, and the maximum efficiency can reach 94.6%. The efficiency of MQBC$_{II}$-VMM$_{II}$ is measured as 93.2% under fully loaded condition, and the maximum efficiency can reach up to 94.1%. The power loss distribution of MQBCI-VMM$_{III}$ and MQBC$_{II}$-VMM$_{II}$ are shown in Fig. 13(b). It can be seen that the power loss of the switch is dominantly high both in MQBC$_{I}$-VMM$_{III}$ and MQBC$_{II}$-VMM$_{II}$, which can be measured as 7.1W and 8.7W, respectively. The power losses of the MOSFET and inductors of MQBC$_{II}$-VMM$_{II}$ are both higher than that of MQBC$_{I}$-VMM$_{III}$, which lead to lower efficiency as compared with MQBC$_{I}$-VMM$_{III}$ by about 0.5%. In addition, since the capacitor C_1 with small rated-voltage and equivalent series resistance is adapted to structure MQBC$_{II}$-VMM$_{II}$, the power loss of the capacitors is lower than that of MQBC$_{I}$-VMM$_{III}$ by 0.7W. The rest of power loss of MQBC$_{I}$-VMM$_{III}$ and MQBC$_{II}$-VMM$_{II}$ is about 0.8W, including PCB and wire conduction loss and so on.

Based on the above experimental results, it can be derived that, each member of this converter family can achieve high voltage gain and possesses different operation performance. One can choose one of these nine converters according to specific application requirement. For example, in addition to high voltage gain, MQBC$_{I}$-VMM$_{III}$ could be selected for utilization as very small input current ripple is required; in consideration of the demand of low buffer capacitor stress, MQBC$_{II}$-VMM$_{II}$ is suggested to be applied and high conversion efficiency can be satisfied at the same time.

VI. CONCLUSIONS

A family of nine high step-up module-integrated converters with dual coupled inductors is proposed in this paper based on the MQBCs and VMMs. These converters can provide high voltage step-up for the power generation systems with low output voltage, such as the PV array and fuel cells system. The operation principle and steady-state performances of the proposed converter family are experimentally verified by taking two cases of $MQBC_{I}$-VMM_{III} and $MQBC_{II}$-VMM_{II} for demonstration. The experimental results shown that high voltage gain can be achieved by adjusting duty cycle and the turn ratios of the coupled inductor of VMM, and the voltage stress across the power switch can be greatly reduced to the value much lower than the output voltage. In addition, this newly proposed converter family can be compatibly integrated in order to achieve high efficiency and small size, and can provide attractive references for new converter design in consideration of renewable energy applications.

REFERENCES

[1] S. S. Thale, R. G. Wandhare, and V. Agarwal, "A novel reconfigurable microgrid architecture with renewable energy sources and storage," *IEEE Trans. Ind. Appl.*, vol. 51, no. 2, pp. 1805–1816, Mar./Apr. 2015.

[2] A. C. Köberle, D. E. H. J. Gernaat, and D. P. van Vuuren, "Assessing current and future techno-economic potential of concentrated solar power and photovoltaic electricity generation," *Energy*, vol. 89, pp. 739–756, Sep. 2015.

[3] R. A. Verzijlbergh, L. J. de Vries, and Z. Lukszo, "Renewable energy sources and responsive demand. Do we need congestion management in the distribution grid?" *IEEE Trans. Power Syst.*, vol. 29, no. 5, pp. 2119–2128, Sep. 2014.

[4] Y.-P. Hsieh, J.-F. Chen, T.-J. Liang, and L.-S. Yang, "Novel high step-up DC-DC converter for distributed generation system," *IEEE Trans. Ind. Electron.*, vol. 60, no. 4, pp. 1473–1482, Apr. 2013.

[5] A. A. A. Freitas, F. L. Tofoli, E. M. Sá Júnior, S. Daher, and F. L. M. Antunes, "High-voltage gain DC-DC boost converter with coupled inductors for photovoltaic systems," *IET Power Electron.*, vol. 8, no. 10, pp. 1885–1892, Oct. 2015.

[6] K.-C. Tseng, C.-C. Huang, and W.-Y. Shih, "A high step-up converter with a voltage multiplier module for a photovoltaic system," *IEEE Trans. Power Electron.*, vol. 28, no. 6, pp. 3047–3057, Jun. 2013.

[7] K.-C. Tseng and C.-C. Huang, "High step-up high-efficiency interleaved converter with voltage multiplier module for renewable energy system," *IEEE Trans. Power Electron.*, vol. 61, no. 3, pp. 1311–1319, Mar. 2014.

[8] F. Evran and M. T. Aydemir, "Isolated high step-up DC-DC converter with low voltage stress," *IEEE Trans. Power Electron.*, vol. 29, no. 7, pp. 3591–3603, Jul. 2014.

[9] T.-J. Liang and J.-H. Lee, "Novel high-conversion-ratio high-efficiency isolated bidirectional DC-DC converter," *IEEE Trans. Ind. Electron.*, vol. 62, no. 7, pp. 4492–4503, Jul. 2015.

[10] Y. Hu, W. Xiao, W. Cao, B. Ji, and D. J. Morrow, "Three-port DC-DC converter for stand-alone photovoltaic systems," *IEEE Trans. Power Electron.*, vol. 30, no. 6, pp. 3068–3076, Jun. 2015.

[11] J.-H. Lee, T.-J. Liang, and J.-F. Chen, "Isolated coupled-inductor-integrated DC-DC converter with nondissipative snubber for solar energy applications," *IEEE Trans. Ind. Electron.*, vol. 61, no. 7, pp. 3337–3348, Jul. 2014.

[12] M. Kim and S. Choi, "A fully soft-switched single switch isolated DC-DC converter," *IEEE Trans. Power Electron.*, vol. 30, no. 9, pp. 4883–4890, Sep. 2015.

[13] T.-J. Liang, J.-H. Lee, S.-M. Chen, J.-F. Chen, and L.-S. Yang, "Novel isolated high-step-up DC-DC converter with voltage lift," *IEEE Trans. Ind. Electron.*, vol. 60, no. 4, pp. 1483–1491, Apr. 2013.

[14] K.-C. Tseng, C.-C. Huang, and C.-A. Cheng, "A high step-up converter with voltage-multiplier modules for sustainable energy applications," *IEEE J. Emerging Sel. Topics Power Electron.*, vol. 3, no. 4, pp. 1100–1108, Dec. 2015.

[15] D. Maksimovic and S. Cuk, "Switching converters with wide DC conversion range," *IEEE Trans. Power Electron.*, vol. 6, no. 1, pp. 151–157, Jan. 1991.

[16] Y.-M. Ye and K. W. E. Cheng, "Quadratic boost converter with low buffer capacitor stress," *IET Power Electron.*, vol. 7, no. 5, pp. 1162–1170, May 2014.

[17] R. Loera-Palomo and J. A. Morales-Saldana, "Family of quadratic step-up DC-DC converters based on non-cascading structures," *IET Power Electron.*, vol. 8, no. 5, pp. 793–801, May 2015.

[18] P. Saadat and K. Abbaszadeh, "A single-switch high step-up DC-DC converter based on quadratic boost," *IEEE Trans. Ind. Electron.*, vol. 63, no. 12, pp. 7733–7742, Dec. 2016.

[19] Y. Tang, T. Wang, and D. Fu, "Multicell switched-inductor/switched-capacitor combined active-network converters," *IEEE Trans. Power Electron.*, vol. 30, no. 4, pp. 2063–2072, Apr. 2015.

[20] G. Wu, X. Ruan, and Z. Ye, "Nonisolated high step-up DC-DC converters adopting switched-capacitor cell," *IEEE Trans. Ind. Electron.*, vol. 62, no. 1, pp. 383–393, Jan. 2015.

[21] J. C. Rosas-Caro, J. C. Mayo-Maldonado, F. Mancilla-David, A. Valderrabano-Gonzalez, and F. B. Carbajal, "Single-inductor resonant switched capacitor voltage multiplier with safe commutation," *IET Power Electron.*, vol. 8, no. 4, pp. 507–516, Apr. 2015.

[22] T. Nouri, S. H. Hosseini, E. Babaei, and J. Ebrahimi, "Generalised transformerless ultra step-up DC-DC converter with reduced voltage stress on semiconductors," *IET Power Electron.*, vol. 7, no. 11, pp. 2791–2805, Nov. 2014.

[23] R. Gules, W. M. dos Santos, F. A. dos Reis, E. F. R. Romaneli, and A. A. Badin, "A modified SEPIC converter with high static gain for renewable applications," *IEEE Trans. Power Electron.*, vol. 29, no. 11, pp. 5860–5871, Nov. 2014.

[24] M. A. H. Al-Saffar and E. Ismail, "A high voltage ratio and low stress DC-DC converter with reduced input current ripple for fuel cell source," *Renew. Energy*, vol. 82, pp. 35–43, Aug. 2015.

[25] L.-W. Zhou, B.-X. Zhu, Q.-M. Luo, and S. Chen, "Interleaved non-isolated high step-up DC/DC converter based on the diode-capacitor multiplier," *Power Electron., IET*, vol. 7, no. 2, pp. 390–397, Feb. 2014.

[26] Y. Deng, Q. Rong, W. Li, Y. Zhao, J. Shi, and X. He, "Single-switch high step-up converters with built-in transformer voltage multiplier cell," *IEEE Trans. Power Electron.*, vol. 27, no. 8, pp. 3557–3567, Aug. 2012.

[27] W. Li, W. Li, X. Xiang, Y. Hu, and X. He, "High step-up interleaved converter with built-in transformer voltage multiplier cells for sustainable energy applications," *IEEE Trans. Power Electron.*, vol. 29, no. 6, pp. 2829–2836, Jun. 2014.

[28] A. Ajami, H. Ardi, and A. Farakhor, "A novel high step-up DC/DC converter based on integrating coupled inductor and switched-capacitor techniques for renewable energy applications," *IEEE Trans. Power Electron.*, vol. 30, no. 8, pp. 4255–4263, Aug. 2015.

[29] S.-W. L. Lee and H.-L. Do, "Zero-ripple input-current high-step-up boost-SEPIC DC-DC converter with reduced switch-voltage stress," *IEEE Trans. Power Electron.*, vol. 32, no. 8, pp. 6170–6177, Aug. 2017.

[30] X. F. Hu and C. Y. Gong, "A high voltage gain DC-DC converter integrating coupled-inductor and diode-capacitor techniques," *IEEE Trans. Power Electron.*, vol. 29, no. 2, pp. 789–800, Feb. 2014.

[31] S. K. Changchien, T. J. Liang, J. F. Chen, and L. S. Yang, "Novel high step-up DC-DC converter for fuel cell energy conversion System," *IEEE Trans. Ind. Electron.*, vol. 57, no. 6, pp. 2007–2017, Jun. 2010.

[32] N. Zhang, D. Sutanto, and K. M. B. Muttaqiand Zhang, "High-voltage-gain quadratic boost converterwith voltage multiplier," *IET Power Electron.*, vol. 8, no. 12, pp. 2511–2519, Jun. 2015.

[33] V. T. Liu and L. J. Zhang, "Design of high efficiency boost-forward-flyback converters with high voltage gain," in *Proc. 11th IEEE Int. Conf. Control Autom.*, Jun. 2014, pp. 1061–1066.

[34] S.-M. Chen, T.-J. Liang, L.-S. Yang, and J.-F. Chen, "A cascaded high step-up DCŰDC converter with single switch for microsource applications," *IEEE Trans. Power Electron.*, vol. 26, no. 4, pp. 1146–1153, Apr. 2011.

[35] A. J. Sabzali, H. M. Behbehani, and E. H. Ismail, "High-voltage step-up integrated double boost-sepic DC-DC converter for fuel-cell and photovoltaic applications," *Renew. Energy*, vol. 82, pp. 44–53, Oct. 2015.

DONGSHENG YU (M'14) received the B.Eng. and Ph.D. degrees from the School of Information and Electrical Engineering, China University of Mining and Technology, Xuzhou, China, in 2005 and 2011, respectively. From 2009 to 2010, he was a Visiting Student with The University of Western Australia, Australia. In 2014, he was an Endeavour Research Fellow with The University of Western Australia. He is currently an Associate Professor with the School of Electrical and Power Engineering, China University of Mining and Technology. His research interests include power electronics, renewable energy, electric drives, nonlinear dynamics, and memristive systems. He has published two books and over 30 papers in these areas.

JIE YANG received the B.Eng. degree from the School of Electronic and Information Engineering, Changchun University, China, in 2014, and the master's degree from the School of Electrical and Power Engineering, China University of Mining and Technology, Xuzhou, China, in 2017. He is currently a Senior Engineer with the State Grid Linyi Power Supply Company, Linyi. His research interests include power electronics, power system, and electric drives.

RUIDONG XU received the B.Eng. and Ph.D. degrees from the School of Information and Electrical Engineering, China University of Mining and Technology, Xuzhou, China, in 2001 and 2012, respectively. In 2001, he joined the School of Information and Electrical Engineering, China University of Mining and Technology as a Lecturer, where he is currently a Professor. His research interests include power electronics, renewable energy, and renewable power generation. He has published over 20 papers in these areas.

ZHENGLONG XIA received the B.Eng. and Ph.D. degrees from the School of Information and Electrical Engineering, China University of Mining and Technology, Xuzhou, China, in 2005 and 2014, respectively. In 2014, he joined the School of Electrical Engineering and Automation, Jiangsu Normal University, as a Lecturer, where he is currently an Associate Professor. His research interests are reactive compensation of power system, fault diagnosis, distributed parallel processing, and neural network. He has published more than 20 research papers in journals.

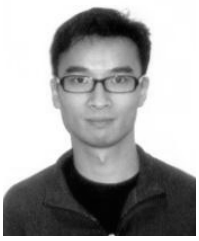

HERBERT HO-CHING IU (S'98–M'00–SM'06) received the B.Eng. degree (Hons) in electrical and electronic engineering from The University of Hong Kong, Hong Kong, in 1997, and the Ph.D. degree from The Hong Kong Polytechnic University, Hong Kong, in 2000.

In 2002, he joined the School of Electrical, Electronic and Computer Engineering, The University of Western Australia, as a Lecturer, where he is currently a Professor. His research interests include power electronics, renewable energy, nonlinear dynamics, current sensing techniques, and memristive systems. He has published over 100 papers in these areas. He received two IET Premium Awards in 2012 and 2014. In 2014, he also received the Vice-Chancellor's Mid-Career Research Award. He currently serves as an Associate Editor for the *International Journal of Bifurcation and Chaos* and the *IEEE Circuits and Systems Society Newsletters* and an Editorial Board Member for the *Australian Journal of Electrical and Electronics Engineering*. He is a Co-Editor of the *Control of Chaos in Nonlinear Circuits and Systems* (Singapore: World Scientific, 2009) and a co-author of the *Development of Memristor Based Circuits* (Singapore: World Scientific, 2013).

TYRONE FERNANDO (SM'05) received the B.Eng. (Hons.) and Ph.D. degrees from the University of Melbourne in 1990 and 1996, respectively. In 1996, he joined The University of Western Australia, School of Electrical Electronic and Computer Engineering, where he is currently a Professor. He was the Deputy Head of the School of Electrical Electronic and Computer Engineering in 2009 and 2010. His research interests include estimations theory, control theory and application of control theory to smart grids, power systems, circuits and systems, and biomedical engineering. He has served as an Associate Editor for the IEEE TRANSACTIONS ON INFORMATION TECHNOLOGY in biomedicine and also as a Guest Editor for the *Journal of the Optimal Control Applications and Methods*. He has authored many journal and conference articles and also two books in the areas of functional observers and closed loop control of blood glucose in diabetics.